High-order harmonic generation and Fano resonances

V. V. Strelkov,[1] M. A. Khokhlova,[1,2] and N. Yu Shubin[3]
[1]*A. M. Prokhorov General Physics Institute, RAS, Moscow, Russia*
[2]*Faculty of Physics, M. V. Lomonosov Moscow State University, Moscow, Russia*
[3]*Scientific Research Institute for System Studies, RAS, Moscow, Russia*
(Received 19 July 2013; published 28 May 2014)

We present a high-order harmonic generation theory which generalizes the strong-field approximation to the resonant case when the harmonic frequency is close to that of the transition from the ground state to an autoionizing state of the generating system. We show that the line shape of the resonant harmonic is a product of the Fano-like factor and the harmonic line which would be emitted in the absence of the resonance. The theory predicts rapid variation of the harmonic phase in the vicinity of the resonance. The calculated resonant harmonic phase is in reasonable agreement with recent measurements. Predicting the phase locking of a group of resonantly enhanced harmonics, our theory allows us to study the perspectives of producing an attosecond pulse train using such harmonics.

DOI: 10.1103/PhysRevA.89.053833 PACS number(s): 42.65.Ky, 32.80.Rm

I. INTRODUCTION

Although high-order harmonic generation (HHG) via interaction of intense laser pulses with matter provides a unique source of coherent femtosecond and attosecond pulses in the extreme ultraviolet (XUV), the low efficiency of the process is a serious limit to its wide application. Using the resonances of the generating medium is a natural way to boost the efficiency, as was already suggested in early HHG experimental [1] and theoretical [2,3] studies. Generation of high harmonics with frequencies close to that of the transition from the ground state to an autoionizing state (AIS) of the generating particle was experimentally investigated in plasma media (for a recent review see [4,5]) and in noble gases [6,7].

A number of theories describing HHG enhancement due to bound-bound transitions were suggested [8–12], and recently, theories based on the specific properties of AIS were developed [13–16]. These theories involve the rescattering model [17,18] in which the HHG is described as a result of tunneling ionization, classical free electronic motion in the laser field, and recombination accompanied by the XUV emission upon the electron's return to the parent ion. In particular, in [16] one of us suggested a four-step resonant HHG model. The first two steps are the same as in the three-step model, but instead of the last step (radiative recombination from the continuum to the ground state) the free electron is trapped by the parent ion, so that the system (parent ion + electron) lands in the AIS, and then it relaxes to the ground state emitting XUV.

In addition, there are several theoretical studies in which the HHG efficiency was calculated using the recombination cross section. It was done heuristically [19] and analytically [20] for the Coulomb interaction and by generalizing the numerical results for the molecules [21].

In this paper we suggest the high-order harmonic generation theory considering an AIS in addition to the ground state and the free continuum treated in the theory for the nonresonant case [22]. We show that such accurate consideration verifies the model [16]. Moreover, we show that the intensity of the resonant HHG is described with a Fano-like factor that includes the scattering cross section. However, in contrast to previously suggested theories, our approach also allows calculating the resonant harmonic's phase.

II. THEORY

We start with the time-dependent Schrödinger equation for an atom or ion in an external laser field linearly polarized along the x axis:

$$i\frac{\partial}{\partial t}\Psi(\mathbf{r},t) = \hat{H}\Psi(\mathbf{r},t), \tag{1}$$

where

$$\hat{H} = -\tfrac{1}{2}\nabla^2 + V(\mathbf{r}) - E(t)x$$

is the total Hamiltonian and $\mathbf{r}$ is the set of coordinate vectors of the electrons in the atom (ion). The wave function can be written as a sum of the ground state, unperturbed continuum, and AIS:

$$\Psi = \Psi_{\text{ground}} + \Psi_{\text{free}} + c(t)\Psi_{\text{AI}}. \tag{2}$$

To solve the Schrödinger equation (1) we use the perturbation method. The wave function obtained in the absence of the AIS in the strong-field approximation (SFA) [22,23] is taken as the unperturbed solution:

$$\Psi_0 = \Psi_{\text{ground}} + \Psi_{\text{free}}.$$

The solution Ψ_0 was found in [22] within the single-electron approximation neglecting the interaction of the free electron with the nucleus and other electrons:

$$\Psi_0(\mathbf{r},t) = e^{iI_p t}\left(a(t)\varphi_{\text{gr}}(\mathbf{r}) + \int d^3\mathbf{v}\, b(\mathbf{v},t)\chi(\mathbf{r})\right), \tag{3}$$

where $\varphi_{\text{gr}}(\mathbf{r})$ is the ground state and $\chi(\mathbf{r})$ is a flat wave. This solution can be generalized to the multielectron case as follows. Let $\mathbf{r}_1$ be the radius vector of the "'active" electron and $\tilde{\mathbf{r}}$ be radius vectors of the other electrons: $\mathbf{r} = \{\tilde{\mathbf{r}},\mathbf{r}_1\}$. Let

$$\chi(\mathbf{r}) = \chi_1(\mathbf{r}_1)\tilde{\varphi}_{\text{gr}}(\tilde{\mathbf{r}})\exp(i\tilde{I}_p t),$$

where $\tilde{I}_p$ is the ionization potential of the *parent ion*. Also, let us write formally

$$V'(\mathbf{r}) = V(\mathbf{r}) - \tilde{V}(\tilde{\mathbf{r}}),$$

where $\tilde{V}(\tilde{\mathbf{r}})$ is the part of the potential which depends only on $\tilde{\mathbf{r}}$. Now the solution $\Psi_0(\mathbf{r},t)$ can be found via a procedure similar to that used in [22]. Namely, neglecting the term $V'(\mathbf{r})\chi(\mathbf{r})$ [but

not the term $\tilde{V}(\tilde{\mathbf{r}})\chi(\mathbf{r})]$ in the Schrödinger equation, we find the equation describing $b(\mathbf{v},t)$ coinciding with Eq. (4) from [22]. Thus the obtained solution satisfies the equation

$$i\frac{\partial}{\partial t}\Psi_0 = \hat{H}\Psi_0 - V'(\mathbf{r})\Psi_{\text{free}}. \tag{4}$$

Neglecting the modification of the AIS by the laser field, the AIS can be written as a solution of the Schrödinger equation:

$$i\frac{\partial}{\partial t}\Psi_{\text{AI}} = \hat{H}(\mathbf{r})\Psi_{\text{AI}}. \tag{5}$$

Since we are planning to calculate the dipole moment of the system which is naturally localized near the origin, below we neglect the outgoing part of this solution and focus on the part localized near the origin. This part can be written using the *complex* energy [24–27]:

$$\Psi_{\text{AI}}(\mathbf{r},t) = \varphi(\mathbf{r})\exp(-iWt). \tag{6}$$

Here $\varphi(\mathbf{r})$ is a stationary solution (in the absence of the configuration interaction, see [28]), and the energy is

$$W = W_0 - i\Gamma/2,$$

where W_0 is the real energy of the AIS and Γ is the AIS width (see [28]),

$$\Gamma = 2\pi|V_1(v_r)|^2, \tag{7}$$

where

$$V_1(\mathbf{v}) = \langle\chi(\mathbf{v})|V'(\mathbf{r})|\varphi\rangle$$

and $v_r = \sqrt{2W_0}$. Note that $\Gamma = 1/\tau$, τ is the lifetime of the AIS.

Using Eqs. (1)–(5), we obtain

$$i\dot{c}\Psi_{\text{AI}} = V'(\mathbf{r})\Psi_{\text{free}}. \tag{8}$$

Multiplying this equation by $\varphi^*(\mathbf{r})$ and integrating over $\mathbf{r}$, we have

$$\dot{c}(t) = -ie^{i(W+I_p)t}\int d^3\mathbf{v}b(\mathbf{v},t)V_1^*(\mathbf{v}). \tag{9}$$

The solution of this equation is

$$c(t) = -i\int_{-\infty}^{t} dt' e^{i(W+I_p)t'}\int d^3\mathbf{v}b(\mathbf{v},t')V_1^*(\mathbf{v}). \tag{10}$$

We can see that the matrix element $V_1(\mathbf{v})$ is the parameter which determines the amplitude of the AIS. Thus this state is a small perturbation of the continuum when this parameter is small (in atomic units). Note that a similar requirement appears in the Fano theory [28] and its applications as the requirement for the resonance to be well isolated in the continuum: $\Gamma \ll W_0$. This condition is usually valid for the autoionizing states of atoms and ions.

Below we find the time-dependent dipole moment of the system:

$$\mu(t) = \langle\Psi(t)|x|\Psi(t)\rangle.$$

Substituting here the wave function given with (2) and neglecting the contribution of the continuum-continuum transitions to the dipole moment (as in [22]) and the contribution of the continuum-AIS transitions to the dipole moment (both assumptions are valid in the case of low population of the continuum), we obtain

$$\mu(t) = \langle\Psi_{\text{ground}}|x|\Psi_{\text{free}}\rangle + \langle\Psi_{\text{ground}}|x|c(t)\Psi_{\text{AI}}\rangle + \text{c.c.} \tag{11}$$

The first term describes HHG in the absence of the resonances of the generating system [see Eq. (6) in [22]]:

$$\mu_{\text{nr}}(t) = \int d^3\mathbf{v}b(\mathbf{v},t)d_{\text{nr}}^*(\mathbf{v}) + \text{c.c.}, \tag{12}$$

where

$$d_{\text{nr}}(\mathbf{v}) = \langle\chi(\mathbf{v})|x|\varphi_{\text{gr}}\rangle$$

is the dipole matrix element of the continuum-ground-state transitions. The second term in Eq. (11) describes the effect of the resonance on the harmonic generation:

$$\mu_r(t) = e^{-i(W+I_p)t}c(t)d_r^* + \text{c.c.},$$

where

$$d_r = \langle\varphi|x|\varphi_{\text{gr}}\rangle$$

is the dipole matrix element of the AIS-ground-state transition. Substituting here Eq. (10), we obtain

$$\mu_r(t) = -id_r^*\int_{-\infty}^{t} dt' e^{i(W+I_p)(t'-t)}\int d^3\mathbf{v}b(\mathbf{v},t')V_1^*(\mathbf{v}) + \text{c.c.}, \tag{13}$$

where $b(\mathbf{v},t')$ (the wave function amplitude of the electron in the free continuum) is the same as that in Lewenstein's theory [see Eq. (5) in [22]].

We transform the Eq. (13) so that it is written using nonresonant contribution (12). We suppose that $V_1^*(\mathbf{v})$ and $d_{\text{nr}}^*(\mathbf{v})$ are smooth functions of the velocity, so they can be taken outside the integral at $v = v_r$. Introducing $\tau' = t - t'$, we have

$$\mu_r(t) = -i\frac{V_1^*(v_r)d_r^*}{d_{\text{nr}}^*(v_r)}\int_0^{\infty} d\tau' e^{-i(W+I_p)\tau'}\mu_{\text{nr}}(t-\tau'). \tag{14}$$

Thus, the spectrum $[f(\omega) = \int_{-\infty}^{\infty} f(t)\exp(i\omega t)dt]$ of the resonant contribution to the dipole moment is

$$\mu_r(\omega) = \frac{V_1^*(v_r)d_r^*}{d_{\text{nr}}^*(v_r)}\frac{\mu_{\text{nr}}(\omega)}{\omega - (W_0+I_p) + i\frac{\Gamma}{2}}, \tag{15}$$

where $\mu_{\text{nr}}(\omega)$ is the spectrum of the nonresonant contribution given by Eq. (8) in [22]. Introducing the detuning from the resonance $\Delta\omega = \omega - (W_0 + I_p)$, we obtain the spectrum of the total dipole moment of the system (11) taking into account (15):

$$\begin{aligned}\mu(\omega) &= \mu_{\text{nr}}(\omega)F(\omega),\\ F(\omega) &= \left[1 + Q\frac{\Gamma/2}{\Delta\omega + i\Gamma/2}\right],\end{aligned} \tag{16}$$

where

$$Q = \frac{V_1^*(v_r)d_r^*}{d_{\text{nr}}^*(v_r)\Gamma/2}. \tag{17}$$

Note that the complex conjugate parameter Q^* is close to the Fano parameter q (which can be real or complex; see [29–31]):

$$Q^* \approx q = \frac{\langle\Phi|x|i\rangle}{\pi V_E^*\langle\psi_E|x|i\rangle}. \tag{18}$$

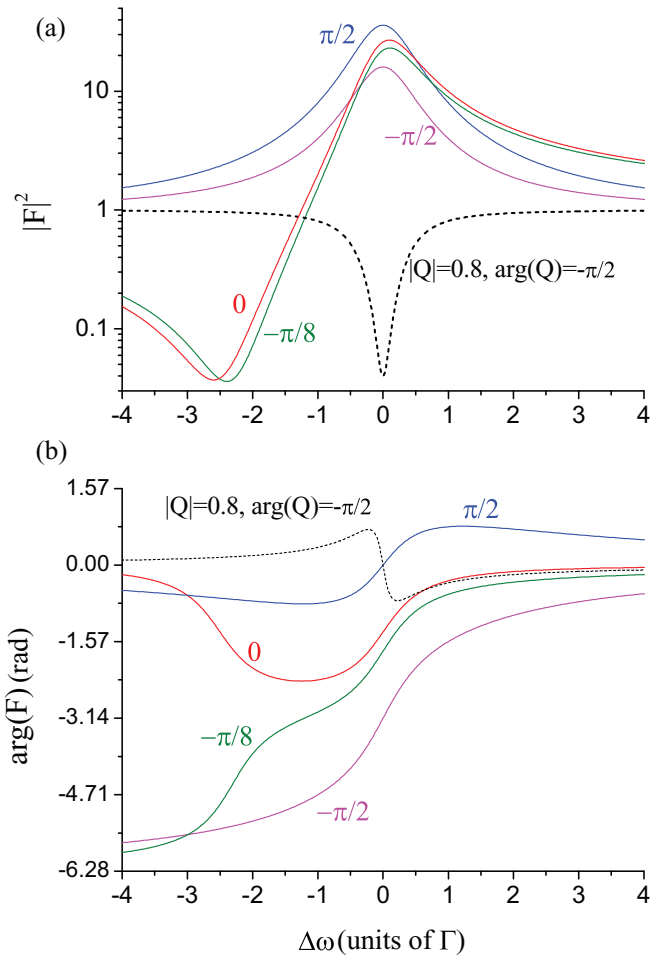

FIG. 1. (Color online) (a) The absolute value squared and (b) the argument of the factor $F(\omega)$ in Eq. (16), calculated for different Q parameters. arg Q is shown near the curves; $|Q| = 5$ for all the curves except the black dashed one.

The approximate character of the equality is due to the following facts: (i) state Φ is different from φ [see Eq. (17) in [28]] and (ii) state ψ_E is different from the free wave χ (see [28] for more details).

The factor $|F(\omega)|^2$ describes the line profile, which coincides with the Fano profile when $Q = q - i$. Note that the phase $2\arg(q - i)$ is introduced in [32] as a characteristic of the process dynamics described by the Fano line. The condition $\Gamma \ll 1$, ensuring the applicability of our approach, in the case of real Q corresponds to $Q \gg 1$; therefore the difference in line shape $|F(\omega)|^2$ from the Fano profile is small in this case.

In Fig. 1 we present the factor $F(\omega)$, calculated for different Q parameters. In Fig. 1 we can see the line asymmetry and a rapid phase variation due to the resonance. Whereas the Fano-like line shape in Fig. 1(a) is, in general, well known, the behavior of the phases was never studied in detail. We can see that in the vicinity of the resonance the phase variation is about π or less; an additional approximately π or $-\pi$ phase advance is either achieved near the minimum of $|F|^2$ [see the asymmetric lines for $\arg(Q) = 0$, $\arg(Q) = -\pi/8$] or distributed at the wings in the case of the symmetric line. In general, essential phase variation can take place not only near the resonance but also far from it. In certain regions of $\arg(Q)$ the phase behavior is extremely sensitive to this value, unlike the line shape [compare cases $\arg(Q) = 0$ and $\arg(Q) = -\pi/8$]. In Fig. 1 we see that for $|Q| = 5$ the phase increases near the resonance for all curves. From Eq. (16) one finds that the slope of the phase at the resonance for high $|Q|$ is approximately the doubled lifetime of the AIS: $\partial[\arg(F)]/\partial\omega \approx 2/\Gamma = 2\tau$. This slope corresponds to the delay in the emission of the resonant harmonic. The presence of this delay confirms the four-step mechanism of the resonant HHG enhancement [16], as first pointed out in the numerical studies [33]. In the opposite case of the window resonance ($|Q| < 1$) the HHG is suppressed, and the slope of the phase is negative (see black dashed curve).

In order to apply Eq. (16) for certain resonances, the complex values of d_r, $d_{\rm nr}$, and V_1 should be known to calculate Q via Eq. (17).

We have $|d_r|^2 = \frac{f_{\rm osc}}{2(I_p+W_0)}$, where $f_{\rm osc}$ is the oscillator strength of the transition. Note that $f_{\rm osc}$ also defines the resonant photorecombination cross section, so our findings in general agree with those in the published studies describing the HHG intensity via the photorecombination cross section [19–21,34].

The matrix element $d_{\rm nr}$ was found in [22] for different binding potentials. Note that the normalization of the free wave in [22,28] is different. If the normalization of [28] is used [providing Eq. (7)], the matrix elements $d_{\rm nr}$ found in [22] should be multiplied by $1/\sqrt{v_r}$.

Finally, $|V_1|^2$ can be found from Γ [see Eq. (7)], which was calculated or measured for many transitions. However, calculating the phase of V_1 is a separate problem which is discussed in the Appendix.

III. RESULTS

In Fig. 2 we present analytical and numerical results of the calculating factor $F(\omega)$ for the transition in Sn^+, which

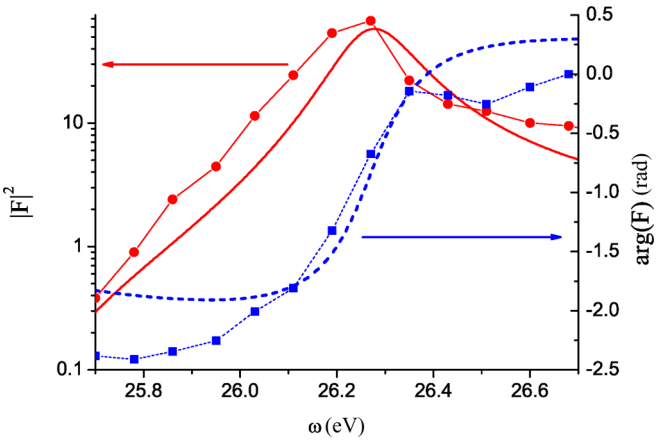

FIG. 2. (Color online) Absolute value squared (solid curves) and argument (dashed curves) of the factor $F(\omega)$, found numerically (curves with symbols) and analytically (curves without symbols) for the $4d^{10}5s^25p\,^2P_{3/2} \leftrightarrow 4d^95s^25p^2(^1D)^2D_{5/2}$ transition in Sn^+; the transition frequency is 26.27 eV, which is close to the 17th harmonic of a Ti:sapphire laser.

is important because of the comparison with experiments discussed below. The approach for calculating $\mu(\omega)$ in the presence of the resonance using the numerical time-dependent Schrödinger equation (TDSE) solution for a model potential is described in [35,36]. However, accurately extracting $F(\omega)$ from this spectrum is an additional problem. To solve it we modify the model potential to *shift* the resonant frequency; the shift is much higher than Γ. Thus in the vicinity of the unshifted resonance shown in Fig. 2 the spectrum calculated with the modified potential $\mu_{\rm mod}(\omega) \approx \mu_{\rm nr}(\omega)$. We are using a generating pulse with a peak intensity of 0.65×10^{14} W/cm^2; the pulse is relatively short (15 fs), so the spectra are quasi-continuous, and F is calculated as $F(\omega) = \mu(\omega)/\mu_{\rm mod}(\omega)$.

Figure 2 shows good agreement between the analytical and numerical results. In the numerically calculated $|F(\omega)|^2$ one can see a small shift of the resonance, which can be attributed to the AIS Stark shift in the laser field. However, neither a broadening of the resonant peak nor a dramatic change of the phase behavior can be seen. Thus one can conclude that neglecting the influence of the laser field on the AIS considered in our theory is a reasonable approximation for resonant HHG in metallic ions. Note that this influence can be important for narrower resonances in He [32,37] and noble gases [38].

High-order harmonic phase measurement for the first time allows direct experimental study of the phase behavior near the Fano resonance. Recently, such a study for HHG from tin plasma under resonant conditions was performed [35] using the reconstruction of attosecond beating by interference of two-photon transitions (RABBIT) technique [39]. It was shown that the resonance considerably changes the relative phase of the neighboring harmonics. The emission time τ_e found with RABBIT for sideband q is linked to phases φ_{q-1} and φ_{q+1} of the two neighboring harmonics as $\tau_e = (\varphi_{q+1} - \varphi_{q-1})/2\omega_0$, where ω_0 is the laser frequency. Thus the change in the emission time due to the resonance is [see Eq. (16)]

$$\Delta\tau_e = \{\arg[F((q+1)\omega_0)] - \arg[F((q-1)\omega_0)]\}/2\omega_0.$$

The emission time calculated with this correction is shown in Fig. 3 together with the experimental and numerical results from [35]. We can see that for the sidebands (SB) far from the resonance (SB12 and SB14) both the theory and the experiment show emission time in agreement with the SFA prediction for the short electronic trajectory, whereas near the resonance (SB16 and SB18) this is not the case. For SB16 our theory agrees with the experiment. The change in τ_e from SB16 to SB18 is negative both experimentally and theoretically, but the measured change is smaller. Most likely, this is so because harmonic 19 is too close to the cutoff and the SFA prediction used in the analytical consideration is not valid. Another probable reason is the influence of the other resonances, which are quite numerous in Sn^+. Note that, experimentally, the RABBIT signal for SB18 was not very stable [35].

In Fig. 4 we present the spectrum of the resonant 17th harmonic calculated using the numerical TDSE solution as described in [35,36] averaged for laser intensities up to 0.8×10^{14} W/cm^2; the laser pulse duration is 50 fs. One can see that different detunings from the resonance lead to different peak harmonic intensities and, even more interesting,

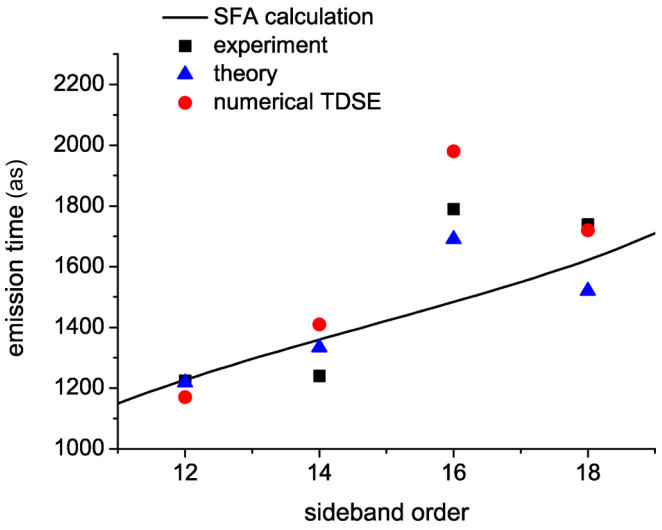

FIG. 3. (Color online) Calculated and measured emission time for high-order harmonics generated in tin plasma plumes. Triangles show calculated results based on the present theory; the other results are from Ref. [35]: dots and squares show the numerical results and those of the RABBIT measurements, respectively, and the black line shows the results of a SFA calculation.

to different harmonic line shapes: for the 793-, 796-, and 808-nm fundamentals the harmonic line consists of two peaks; it is known for the nonresonant HHG that these peaks can be attributed to the contributions of the short and the long electronic trajectories (see [40] and references therein). In Fig. 4 we can see that the long trajectory's contribution is, in general, weak, but it becomes more pronounced when its frequency is closer to the exact resonance, as is the case for the 793-nm fundamental. These results illustrate the fact that the harmonic line shape can be well understood via the factorization of the harmonic signal described by Eq. (16). This straightforward factorization is a remarkable fact, considering the complexity of the dynamics of *both* the free electronic wave packet and the AIS, which determine the harmonic line shape.

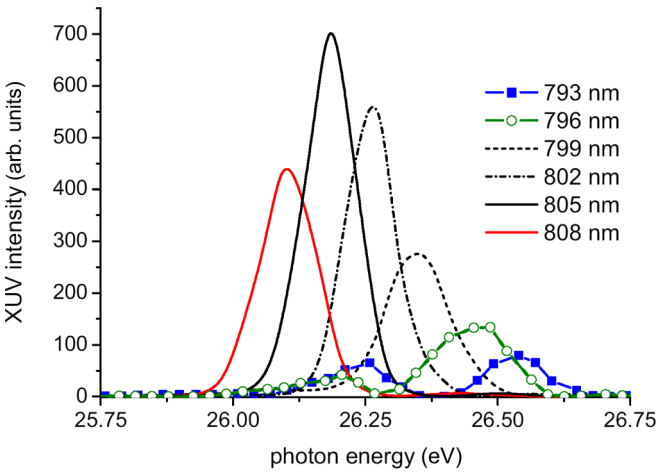

FIG. 4. (Color online) The calculated harmonic spectrum in the vicinity of the resonance for different fundamental wavelengths, leading to different detunings from the resonance. The resonant transition is the same as in Fig. 2.

IV. DISCUSSION AND CONCLUSIONS

The harmonic phase variation due to the factor $F(\omega)$ in the vicinity of a wide (i.e., covering several harmonics) resonance can be used for compensation of the attochirp (variation of τ_e as a function of the harmonic order). Namely, for the resonant harmonics *above* the resonance the attochirp is compensated for by the short electronic trajectory, and for those *below* the resonance it is compensated for by the long one. The variation of the additional emission time is $\partial\Delta\tau_e/\partial\omega = \partial^2 \arg[F(\omega)]/\partial\omega^2 \sim 1/\Gamma^2$. This estimate shows that, in particular, resonant HHG in Xe using a 1–2-μm pump is a good candidate for attochirp compensation via the resonance in Xe at approximately 100 eV.

Above we have considered a single AIS. However, our perturbation theory can be easily generalized for the case of multiple nonoverlapping autoionizing (AI) states, keeping the assumption that the influence of these states on the free electronic wave packet Ψ_{free} remains small. Namely, to take into account several AISs, the terms corresponding to each state with its specific Q, $\Delta\omega$, and Γ should be added in the brackets in the right part of Eq. (16).

In conclusion, in this paper we present a theory which generalizes the SFA approach for HHG to the resonant case, considering an AIS in addition to the ground state and the free continuum state; the latter two states are treated in the same way as in the theories developed for the nonresonant case. The main result is given by Eq. (16), which presents the resonant harmonic line as a product of the Fano-like factor and a harmonic line which would be emitted in the absence of the AIS. Our theory allows calculating not only the resonant harmonic intensity but also its phase. We show that there is a rapid variation of the phase in the vicinity of the resonance. Our calculations reasonably agree with the RABBIT harmonic phase measurements. Our theory predicts that in the case of a resonance covering a group of harmonics the resonance-induced phase variation can compensate for the attochirp in a certain spectral region. The natural progression of our studies would be to take into account the influence of the laser field on the AIS.

ACKNOWLEDGMENTS

The authors acknowledge fruitful discussions with D. Kilbane, M. Fedorov, A. Magunov, and P. Saliéres. This study was supported by RFBR (Grants No. 12-02-00627-a and No. 13-02-92623) and the Dynasty Foundation.

APPENDIX

Calculating the complex matrix element V_1 is a very complex problem even for simple multielectronic systems. Here we suggest a single-electron model where this matrix element can be found exactly. Note that neither our approach nor the Fano theory specifies the nature of the potential $V'(\mathbf{r})$ in (4): the potential can include the electron-electron interaction (as in the case of AI state), but it can be some model potential as well.

To find the matrix element

$$V_1(\mathbf{v}) = \langle\chi(v_r)|V'(r)|\varphi_{\text{qs}}\rangle$$

we use the fact that $V'(x) = \hat{H} + \frac{1}{2}\nabla^2$. Then $V_1(v_r) = W\langle\chi(v_r)|\varphi_{\text{qs}}\rangle + \langle\chi(v_r)|\frac{1}{2}\nabla^2|\varphi_{\text{qs}}\rangle$. Further we present the AIS at $+\infty$ as an outgoing wave,

$$\varphi_{\text{qs}} = Ae^{i\theta}\chi(v_r), \tag{A1}$$

and take into account that φ_{qs} is either symmetric or antisymmetric and that the total flux of the AIS wave function over the integration boundary which is far from the origin is $2A^2v_r$. Then upon integration of $\langle\chi(v_r)|\frac{1}{2}\nabla^2|\varphi_{\text{qs}}\rangle$ twice by parts we obtain

$$V_1(v_r) = W\langle\chi(v_r)|\varphi_{\text{qs}}\rangle + iA\sqrt{v_r}e^{i\theta} - \frac{v_r^2}{2}\langle\chi(v_r)|\varphi_{\text{qs}}\rangle,$$

where $W = W_0 - i\Gamma/2 = v_r^2/2 - i\Gamma/2$. Then we find

$$V_1(v_r) = iA\sqrt{v_r}e^{i\theta} - i\Gamma\langle\chi(v_r)|\varphi_{\text{qs}}\rangle/2. \tag{A2}$$

The total flux of the AIS wave function equals Γ (see [41]); thus $A = \sqrt{\frac{\Gamma}{2v_r}}$. Now we can see that the first term in (A2) is proportional to $\sqrt{\Gamma}$, whereas the second one is proportional to Γ, and thus the latter can be neglected for small Γ. So, finally, we have $V_1(v_r) = i\sqrt{\frac{\Gamma}{2}}e^{i\theta}$.

To find θ we use a model potential which has a ground state and a single quasistationary state φ_{qs}, with the latter corresponding to the AIS in the real system. A one-dimensional double-barrier structure with a gap between the barriers (see Fig. 5) can reproduce well the essential features of the generating system. The exact choice of the parameters of this model potential (so that the energy of the quasistationary state and its lifetime and the energy of the ground state fit those of the real ion) is described below. This model allows us to solve the Schrödinger equation without the laser field analytically.

We find the wave function between the barriers in the model potential using the analogy with electromagnetic field in a Fabry-Pérot interferometer. Between the barriers the wave experiences multiple reflections from the two barriers. We

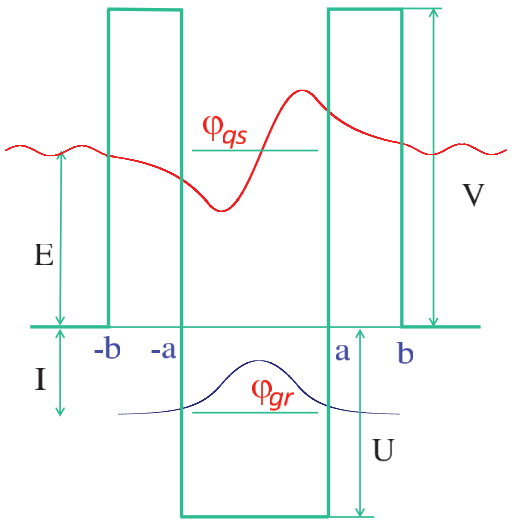

FIG. 5. (Color online) The model double-barrier potential with a gap between the barriers. There are the ground state φ_{gr} and the quasistationary state φ_{qs}, which reproduces the AI state in the real atom (or ion).

look for a solution corresponding to the incident wave of unit amplitude. Thus the wave function between the barriers can be written in the form

$$\varphi_{\rm qs} = [C_1 \exp(ik'x) + C_2 \exp(-ik'x)] \exp(i\xi), \qquad \text{(A3)}$$

where $k' = \sqrt{2(U+E)}$ is the wave number in the region between the barriers, E is the incident wave energy, and ξ is a phase chosen so that the matrix element d_r is real. Note that the wave function in the form (A3) contains an outgoing wave at $+\infty$ outside the barrier as in (A1).

C_1 and C_2 can be found as

$$C_1 = \frac{\sqrt{D}\exp(i\phi_d)}{1 - R\exp(2i\phi_r)}, \quad C_2 = \frac{\sqrt{DR}\exp[i(\phi_r+\phi_d)]}{1 - R\exp(2i\phi_r)}. \qquad \text{(A4)}$$

Here D and R are the transition and reflection coefficients for the amplitude, respectively, and ϕ_d and ϕ_r are the phase shifts that the wave function acquires upon transition and reflection in the case of a single barrier. These factors have the following form:

$$\begin{aligned}
D &= \frac{4v^2\kappa^2}{(\kappa^2 - vk')^2 \sinh^2[\kappa(b-a)] + \kappa^2(v+k')^2\cosh^2\kappa(b-a)},\\
R &= \frac{(\kappa^2 + vk')^2 \sinh^2[\kappa(b-a)] + \kappa^2(v-k')^2\cosh^2\kappa(b-a)}{(\kappa^2 - vk')^2 \sinh^2[\kappa(b-a)] + \kappa^2(v+k')^2\cosh^2\kappa(b-a)},\\
\phi_d &= \arctan\left(\frac{vk'-\kappa^2}{(v+k')\kappa}\tanh[\kappa(b-a)]\right) - vb + k'a,\\
\phi_r &= \arctan\left(-\frac{2k'\kappa(v^2+\kappa^2)\coth\kappa(b-a)}{v2k'^2 - \kappa^4 + \kappa^2(v^2-k'^2)\coth^2[\kappa(b-a)]}\right) + 2k'a + \ pi,
\end{aligned} \qquad \text{(A5)}$$

where v is the velocity of the incident wave with energy E and $\kappa = \sqrt{2(V-E)}$.

Let us consider the dipole matrix element of the ground-state–quasistationary-state transition defined as $\tilde{d}_r = \langle\varphi_{\rm qs}\exp(-i\xi)|x|\varphi_{\rm gr}\rangle = d_r\exp(i\xi)$. We assume the ground state $\varphi_{\rm gr}$ coincides with the ground state of the infinitely deep potential gap as $\varphi_{\rm gr} = \frac{1}{\sqrt{a}}\cos(qx)$, where $q = \frac{\pi}{2a}$ is the wave number corresponding to the ionization potential of the generating system (because in this case the barrier is high and the tunneling probability is very low). Using the quasistationary-state wave function (3), we find the dipole matrix element $\tilde{d_r}^*$ of the ground-state–quasistationary-state transition as

$$\tilde{d_r}^* = \frac{\sqrt{D}\exp(i\phi_d)}{1+\sqrt{R}\exp(i\phi_r)}(A-B), \qquad \text{(A6)}$$

where

$$\begin{aligned}
A &= \frac{1}{\sqrt{a}}\left(\frac{\sin(k'+q)a}{(k'+q)^2} + \frac{\sin(k'-q)a}{(k'-q)^2}\right),\\
B &= \sqrt{a}\left(\frac{\cos(k'+q)a}{k'+q} + \frac{\cos(k'-q)a}{k'-q}\right).
\end{aligned}$$

Since we have defined d_r as being real, then it is equal to the absolute value of $\tilde{d_r}^*$; therefore the phase ξ in (A3) can be found as $\arg(-\tilde{d_r}^*)$. Thus for the considered double-barrier model we can obtain the phase ξ in the following form:

$$\xi = \arctan\left(\frac{\sqrt{R}\sin\phi_r}{1+\sqrt{R}\cos\phi_r}\right) - \phi_d. \qquad \text{(A7)}$$

On the one hand, we can obtain the wave function $\varphi_{\rm qs}$ at $+\infty$ as a plane wave between the barriers propagating to the right in (A3) with the amplitude changed by a factor of $\sqrt{D}$ and acquiring the phase shift ϕ_d after tunneling through the barrier. Thus the phase at $+\infty$ can be found as $\arg(C_1) + \xi + \phi_d$, where $\arg(C_1) = \phi_d + \arctan(\frac{R\sin 2\phi_r}{1-R\cos 2\phi_r})$ and ξ is defined in (A7). On the other hand, the wave function outside the barrier can be presented as in (A1). Comparing the phase of the wave function $\varphi_{\rm qs}$ at $+\infty$ in these two cases, we obtain the phase θ in the following form:

$$\begin{aligned}
\theta = \phi_d &+ \arctan\left(\frac{R\sin 2\phi_r}{1 - R\cos 2\phi_r}\right)\\
&+ \arctan\left(\frac{\sqrt{R}\sin\phi_r}{1+\sqrt{R}\cos\phi_r}\right),
\end{aligned} \qquad \text{(A8)}$$

where the parameters R, ϕ_r, ϕ_d, defined by (A5), are calculated by substituting the AIS energy for that of the quasistationary state in our model.

We used the following considerations for choosing the parameters of the model potential shown in Fig. 5. The population in the region between the barriers $[\int_{-a}^{a}|\varphi_{\rm qs}|^2dx$, where $\varphi_{\rm qs}$ is determined by formula (A3)] has maxima corresponding to quasistationary states. The parameters a, b, V, and U of the model potential were chosen so that there are two states in it and, moreover, the energy and width of the quasistationary state, the ground-state energy, and the oscillator strength of the quasistationary-state–ground-state transition coincide with those of the real ion. Thus the quasistationary (autoionizing) state energy should be equal to $W_0 = \frac{v_r^2}{2}$. The procedure for finding the parameters was as follows. First, the parameters of the finite-depth gap (V and a) corresponding to the real values of the energy difference between the ground state and the AIS and the oscillator strength were found by the gradient descent method. Then, U was selected so that the absolute value of the ground-state energy equals the ionization potential of the real system. Finally, parameter b was found so that the quasistationary-state width in the model potential coincides with that of the AI state of the ion.

[1] E. Toma, Ph. Antoine, A. de Bohan, and H. Muller, J. Phys. B **32**, 5843 (1999).
[2] L. Plaja and L. Roso, J. Mod. Opt. **40**, 793 (1993).
[3] P. A. Oleinikov, V. T. Platonenko, and G. Ferrante, J. Exp. Theor. Phys. Lett. **60**, 246 (1994).
[4] R. A. Ganeev, J. Mod. Opt. **59**, 409 (2012).
[5] R. A. Ganeev, *High-Order Harmonic Generation in Laser Plasma Plumes* (Imperial College Press, London, 2012).
[6] S. Gilbertson, H. Mashiko, Ch. Li, E. Moon, and Z. Chang, Appl. Phys. Lett. **93**, 111105 (2008).
[7] A. D. Shiner *et al.*, Nat. Phys. **7**, 464 (2011).
[8] C. Figueira de Morisson Faria, R. Kopold, W. Becker, and J. M. Rost, Phys. Rev. A **65**, 023404 (2002).
[9] R. Taieb, V. Veniard, J. Wassaf, and A. Maquet, Phys. Rev. A **68**, 033403 (2003).
[10] M. B. Gaarde and K. J. Schafer, Phys. Rev. A **64**, 013820 (2001).
[11] M. Plummer and C. J. Noble, J. Phys. B **35**, L51 (2002).
[12] K. Ishikawa, Phys. Rev. Lett. **91**, 043002 (2003).
[13] D. Milošević, J. Phys. B **40**, 3367 (2007).
[14] M. V. Frolov, N. L. Manakov, T. S. Sarantseva, M. Y. Emelin, M. Y. Ryabikin, and A. F. Starace, Phys. Rev. Lett. **102**, 243901 (2009).
[15] I. A. Ivanov and A. S. Kheifets, Phys. Rev. A **78**, 053406 (2008).
[16] V. Strelkov, Phys. Rev. Lett. **104**, 123901 (2010).
[17] P. B. Corkum, Phys. Rev. Lett. **71**, 1994 (1993).
[18] K. J. Schafer, B. Yang, L. F. DiMauro, and K. C. Kulander, Phys. Rev. Lett. **70**, 1599 (1993).
[19] V. T. Platonenko, Quantum Electron. **31**, 55 (2001).
[20] M. V. Frolov, N. L. Manakov, T. S. Sarantseva, and A. F. Starace, Phys. Rev. A **83**, 043416 (2011).
[21] T. Morishita, A.-T. Le, Z. Chen, and C. D. Lin, Phys. Rev. Lett. **100**, 013903 (2008).
[22] M. Lewenstein, P. Balcou, M. Y. Ivanov, A. L'Huillier, and P. B. Corkum, Phys. Rev. A **49**, 2117 (1994).
[23] L. V. Keldysh, Zh. Eksp. Teor. Fiz. **47**, 1945 (1964) [Sov. Phys. JETP **20**, 1307 (1965)].
[24] Ya. B. Zel'dovich, Zh. Eksp. Teor. Fiz. **39**, 776 (1960) [Sov. Phys. JETP **12**, 542 (1961)].
[25] S. T. Manson, Phys. Rev. **145**, 35 (1966).
[26] Th. Mercouris and C. A. Nicolaides, J. Phys. B **30**, 811 (1997).
[27] Ph. Durand and I. Paidarova, J. Phys. B **46**, 075001 (2013).
[28] U. Fano, Phys. Rev. **124**, 1866 (1961).
[29] N. L. S. Martin, B. A. deHarak, and K. Bartschat, J. Phys. B **42**, 225201 (2009).
[30] K. Kobayashi, H. Aikawa, S. Katsumoto, and Y. Iye, Phys. Rev. B **68**, 235304 (2003).
[31] M. Wickenhauser, J. Burgdorfer, F. Krausz, and M. Drescher, Phys. Rev. Lett. **94**, 023002 (2005).
[32] C. Ott, A. Kaldun, P. Raith, K. Meyer, M. Laux, J. Evers, C. H. Keitel, C. H. Greene, and T. Pfeifer, Science **340**, 716 (2013).
[33] M. Tudorovskaya and M. Lein, Phys. Rev. A **84**, 013430 (2011).
[34] S. Patchkovskii, O. Smirnova, and M. Spanner, J. Phys. B **45**, 131002 (2012).
[35] S. Haessler *et al.*, New J. Phys. **15**, 013051 (2013).
[36] R. A. Ganeev, V. V. Strelkov, C. Hutchison, A. Zaïr, D. Kilbane, M. A. Khokhlova, and J. P. Marangos, Phys. Rev. A **85**, 023832 (2012).
[37] J. Zhao and M. Lein, New J. Phys. **14**, 065003 (2012).
[38] H. Wang, M. Chini, S. Chen, C.-H. Zhang, F. He, Y. Cheng, Y. Wu, U. Thumm, and Z. Chang, Phys. Rev. Lett. **105**, 143002 (2010).
[39] P. M. Paul, E. Toma, P. Breger, G. Mullot, F. Auge, P. Balcou, H. Muller, and P. Agostini, Science **292**, 1689 (2001).
[40] A. Zair *et al.*, Phys. Rev. Lett. **100**, 143902 (2008).
[41] L. D. Landau and E. M. Lifshitz, *Quantum Mechanics* (Pergamon, Oxford, 1977), Sec. 134.